Exosome-Mediated mRNA Delivery For SARS-CoV-2 Vaccination

[1]Shang Jui Tsai, [1]Chenxu Guo, [2]Alanna Sedgwick, [2]Saravana Kanagavelu, [2]Justin Nice, [2]Sanjana Shetty, [2]Connie Landaverde, [2]Nadia A. Atai, and [1]*Stephen J. Gould

[1]Department of Biological Chemistry, The Johns Hopkins University School of Medicine, 725 North Wolfe Street, Baltimore, MD, 21205

[2]Capricor Therapeutics, Inc. 8840 Wilshire Blvd. 2nd Floor, Beverly Hills, CA 90211

Correspondence:

Name: Stephen J. Gould

Address: 725 North Wolfe Street
Physiology Building, Room 409
Baltimore, MD 21205
USA

Phone number: 443 847 9918

Email: sgould@jhmi.edu

Running title: Exosomal SARS-CoV-2 vaccine

Key Words: COVID19, spike, nucleocapsid, exosomes, mRNA, lipid, antibody, T-cell, extracellular vesicles

Abstract

Expression-dependent, Spike-only vaccines have been developed, deployed, and shown to be effective in the fight against SARS-CoV-2. However, additional approaches to vaccine development may be needed to meet existing and future challenges posed by emerging Spike variant strains, as well as a likely need for different antigen-delivery systems that are safe and effective for regular, periodic re-administration. We report here the development of mRNA-loaded exosomes, demonstrate that they can mediate the functional expression of heterologous proteins *in vitro* and *in vivo*, and have fewer adverse effects than comparable doses of lipid nanoparticles. Furthermore, we applied this approach to the development of an exosome-based, multiplexed mRNA vaccine that drives expression of immunogenic SARS-CoV-2 Nucleocapsid and Spike proteins. This vaccine elicited long-lasting cellular and humoral responses to Nucleocapsid and to Spike, demonstrating that exosome-based mRNA formulations represent a previously unexplored platform in the fight against COVID-19 and other infectious diseases.

Introduction

Severe acute respiratory syndrome coronavirus 2 (SARS-CoV-2) is the causative agent of COVID-19 [1,2]. COVID-19 typically presents with symptoms common to many respiratory infections, including fever and cough, but in many cases progresses to more severe disease that may include acute respiratory distress, disseminated disease, and death [34-8]. SARS-CoV-2 entered the human population in late 2019 as the result of a zoonotic leap and is most closely related to coronaviruses endemic to bats (Chiroptera) [9]. SARS-CoV-2 is the third recent zoonotic betacoronavirus to enter the human population, the others being responsible for the outbreaks of severe acute respiratory syndrome (SARS-CoV) in 2002 [10] and middle east respiratory syndrome (MERS-CoV) in 2012 (Memish et al., 2013), indicative of a generally susceptibility of human populations to coronavirus zoonoses. These zoonoses are more distantly to human endemic betacoronaviruses (OC43, HKU1, etc.) that also cause respiratory infections of milder effect [11]). While SARS-CoV-2 infection is associated with lower mortality than SARS-CoV or MERS-CoV, SARS-CoV-2 initially displayed a higher rate of transmission, quickly became a major cause of morbidity and mortality worldwide (https://www.cdc.gov/coronavirus/2019-ncov/hcp/clinical-guidance-management-patients.html)(coronavirus.jhu.edu), and has continued to evolve into numerous variant strains that display even more-elevated rates of transmission and an emerging resistance to antibody-based neutralization [12-15].

SARS-CoV-2 enters host cells via a multistep pathway that begins with binding between the Spike protein on the virus surface and its cognate receptor proteins on the host cell

surface. These include angiotensin-converting enzyme II (ACE2) [1,16,17], neuropilin-1 [18,19], and perhaps also CD147 [20]. Following virus-cell binding, host cell proteases (e.g. TMPRSS2 [16], cathepsins [21], etc.) cleave Spike, potentiating Spike-catalyzed fusion between the viral and cellular membranes and functional infection of the host cell. Not surprisingly, SARS-CoV-2 receptors and proteases are expressed within the respiratory tract, consistent with its respiratory mode of transmission [22]. However, they are also expressed in many other cell types, allowing SARS-CoV-2 to spread within the body and impact multiple organ systems (brain, heart, gastrointestinal tract, circulatory system, immune system, etc. [18,19,23-26]).

Following virus-cell membrane fusion, the viral genomic RNA (gRNA) is translated to generate two large polyproteins, open reading frame 1 (orf1a) and orf1ab, which are processed to release 16 nonstructural proteins (nsp1-16) [27]. These early proteins prime the host cell for virus replication and mediate the synthesis of subgenomic viral RNAs and their unique protein products. These include a dozen or more additional proteins, including the SARS-CoV-2 structural proteins Nucleocapsid (N), Spike (S), Membrane (M), and Envelope (E). Spike, Membrane and Envelope are integral membrane proteins, co-translationally translocated into the endoplasmic reticulum (ER), that subsequently drive virion formation while also incorporating the Nucleocapsid and its bound gRNA as well as some other ancillary proteins [28,29], with virus release via lysosomal exocytosis (Ghosh et al., 2020) []. The released viral particles are ~100 nm diameter, display prominent Spike protrusions from the cell surface and a lumen containing Nucleocapsid-gRNA complexes[30]. SARS-CoV-2 biogenesis also involves extensive processing of its

87 Spike protein at a polybasic site, generating S1 and S2 forms of Spike, with the N-
88 terminal, receptor-binding S1 fragment bound non-covalently to the fusogenic,
89 membrane-anchored S2 fragment [16,31,32].
90
91 Vaccine design should mirror, and ideally improve on, the correlates of protective
92 immunity that arise from natural infections. It is now well-established that SARS-CoV-2
93 infection generates potent cellular and humoral immune responses to viral proteins that
94 in most cases reverse the course of disease, clear the viral infection, and confer
95 resistance to reinfection in both people and in animal models [33-3637-39]. Disease-preventing
96 vaccines have previously been developed for animal coronaviruses [40] and have been
97 successfully developed and deployed for SARS-CoV-2 [41-47], a development that is likely
98 to save millions of lives. However, these first-generation SARS-CoV-2 vaccines only elicit
99 immunity to a single viral protein, Spike, the rapid evolution of which may impair vaccine
100 efficacy [12-15]. Furthermore, the Spike-only vaccine approach ignores the fact that a
101 primary correlate of immunity in COVID-19 patients is the array of potent immune
102 reactions to the SARS-CoV-2 Nucleocapsid protein [48].
103
104 Here we describe an expression-dependent SARS-CoV-2 vaccine that combines
105 exosome-based delivery, multiplexed mRNA formulation, induction of immunity to both
106 Spike and Nucleocapsid, and antigen design that involves expressing Nucleocapsid in a
107 form designed for improved antigen presentation. Exosomes are small extracellular
108 vesicles (sEVs) of ~30-150 nm in diameter that are made by all cells, abundant in all
109 biofluids, and mediate intercellular transmission of signals and macromolecules, including

110 RNAs [49]. Allogenic exosome transplantations and transfusions have been practices in
111 one form or another for more than a century and have never been associated with any
112 adverse effects. Moreover, exosomes have already been shown effective for delivery of
113 RNA-based therapeutics [50,51]. The remainder of this report describes the production of
114 engineered exosome/mRNA formulations, their ability to drive protein expression in
115 cultured cells and animals, their improved safety relative to LNPs, and their use as a
116 multiplexed, exosome-based SARS-CoV-2 vaccine that elicited immunity to multiple viral
117 antigens, including Nucleocapsid as well as Spike.
118

Results

Exosomes display robust ability to deliver functional mRNAs in vitro and in vivo

Exosomes are capable of delivering functional RNAs to target cells [50,51], but so too are synthetic lipid vesicles, often referred to as lipid nanoparticles (LNPs) [52]. To better understand the dynamics of mRNA delivery by these two natural and synthetic forms of soluble vesicles, we generated matched formulations of mRNA-loaded exosomes and mRNA-loaded LNPs. Exosomes were purified from the culture of 293F cells (***Fig. 1***), LNPs [52] were obtained from a commercial provider, and equal amounts of each (by vesicle number) were loaded with a synthetic mRNA encoding the hybrid luciferase/fluorescent protein Antares2 (Antares2 is comprised of the luciferase teLuc fused to two copies of the fluorescent protein CyOFP1 (CyOFP1-teLuc-CyOFP1), emits far-red shift light via bioluminescent resonance energy transfer[53]). Equal amounts of these matched exo-mRNA and LNP-mRNA formulations were then incubated at low and high doses with human cells, followed by an overnight incubation to allow for Antares2 protein expression. The next day, the cells were incubated with diphenylterazine (DTZ), a cell-permeable substrate (luciferin) for Antares2, and assayed for DTZ-dependent, Antares2-catalyzed light emission (***Fig. 2***). At low-dose administration, Antares2 expression was 25% higher in cells treated with the exo-mRNA formulation than with the LNP-mRNA formulation (n = 6, p = 0.0016). The difference in Antares2 expression was even more pronounced at high-dose administration, as the exo-mRNA-treated cells expressed far more Antares2 activity than the LNP-exo-treated cells (16-fold; n = 6; p = 0.00035).

141 This large difference in particle-mediated Antares2 expression was caused by a drop in
142 LNP-mRNA-mediated expression, raising the possibility that LNP administration is
143 inhibitory at high levels of administration. This in turn raised the possibility of general
144 toxicity of LNP administration, which we addressed by following the short-term
145 consequences of exosome and LNP injections in mice. Animals were injected (i.m.) with
146 equal numbers of either exosomes or LNPs (50 ml of ??? particles/ml), returned to their
147 cages for three days, and then sacrificed and processed for organ histology by an
148 independent testing laboratory (***Fig. 3A***). No abnormalities were detected in control
149 animals (5/5) or in animals injected with exosomes (5/5). In contrast, only one of the LNP-
150 injected animals (1/5) displayed normal spleen histology, as 4/5 animals showed an
151 increase in red pulp. Adverse LNP effects may also explain the ~5% reduction in body
152 mass (n = 5; p = 0.05) we observed at 3 days post-injection (***Fig. 3B***).
153
154 The robust expression of exosome-delivered mRNA *in vitro* and the absence of exosome-
155 associated adverse effects led us to next test whether RNA-loaded exosomes might also
156 be able to drive Antares2 expression *in vivo*. Towards this end, we injected adult mice
157 (0.05 ml volume, intramuscular (i.m.) administration) with Antares2 mRNA-loaded
158 exosomes, returned the animals to cages to allow for Antares2 expression. 24 hours later,
159 the control (uninjected) and treated mice were injected (i.p.) with a solution of the
160 Antares2 luciferin DTZ and imaged immediately using a real-time bioluminescent imaging
161 (BLI) system to visualize exosome-mediated, mRNA-directed Antares2 expression.
162 Control animals displayed no significant light emission upon DTZ injections whereas
163 animals that had been injected with the mRNA-loaded exosome formulation displayed

164 robust light emission (***Fig. 3***). These observations demonstrate that RNA-loaded
165 exosomes can deliver functional mRNAs into cells in live animals in a way that leads to
166 mRNA translation, protein expression, and directed enzyme activity.
167

168 ***Design and validation of S^{W1} and LSNME mRNAs***

169 We next tested whether exosome-mRNA formulations can be used to elicit immune
170 responses to mRNA-encoded antigens. Towards this end, we synthesized a pair of
171 mRNAs, one of which expresses the form of SARS-CoV-2 Spike (S^{W1}) encoded by the
172 initial viral isolate [1]. The second mRNA expresses a fusion protein (LSNME) comprised
173 of the SARS-CoV-2 Nucleocapsid protein, as well as fragments of the Spike, Membrane,
174 and Envelope proteins, all inserted in the extracellular domain of human Lamp1 (this
175 Lamp1-based fusion protein aims to induce anti-SARS-CoV-2 immunity by targeting viral
176 protein fragments to the MHC Class I and II antigen presentation pathways [54,5556]).
177 Transfection of these mRNAs into HEK293 cells (***Fig. 4***) resulted in expression of Spike
178 at the cell surface but also at internal organelles (shown elsewhere to be lysosomes [57]),
179 whereas expression of LSNME led to its accumulation in what appears to the
180 endoplasmic reticulum, the site of MHC Class I peptide loading and maturation.
181

182 ***The LSNME/S^{W1} vaccine induces antibody responses to N and S***

183 A single exosome-mRNA formulation containing both the LSNME and S^{W1} mRNAs
184 (hereafter referred to as the LSNME/S^{W1} vaccine) was injected (i.m.) into 13 weeks-old
185 male C57BL/6J mice (***Fig. 5***). The vaccine was dosed at 4 ug or 0.25 ug equivalents of
186 each mRNA and injections were performed on day 1 (primary immunization), day 21 (1st

187 boost), and day 42 (2nd boost). Blood (0.1 mL) was collected on days 14, 35, 56, 70 and
188 84. On day 84 the animals were sacrificed to obtain tissue samples for histological
189 analysis and splenocytes for blood cell studies. Using ELISA kits adapted for the detection
190 of mouse antibodies, we observed that vaccinated animals displayed a dose-dependent
191 antibody response to both the SARS-CoV-2 N protein and S protein. These antibody
192 reactions were not particularly robust but they were long-lasting, persisting to 7 weeks
193 after the final boost with little evidence of decline. It should be noted that the modest
194 antibody production was expected in the case of the N protein, as the LSNME mRNA is
195 designed to stimulate cellular immune responses rather than the production of anti-N
196 antibodies.
197
198 ***LSNME/S^{W1} vaccination induces cellular immune responses to N and S***
199 Vaccinated and control animals were also interrogated for the presence of antigen-
200 reactive CD4+ and CD8+ T-cells. This was carried out by collecting splenocytes at the
201 completion of the trial (day 84) using a CFSE proliferation assay in the presence or
202 absence of recombinant N and S proteins. These experiments revealed that vaccination
203 had induced a significant increase in the percentages of CD4$^+$ T-cells and CD8$^+$ T-cells
204 that proliferated in response to addition of either recombinant N protein or recombinant S
205 protein to the culture media (***Fig. 6A-D***). These vaccine-specific, antigen-induced
206 proliferative responses demonstrate that the LSNME/S^{W1} vaccine achieved its primary
207 goal, which was to prime the cellular arm of the immune system to generate N-reactive
208 CD4$^+$ and CD8$^+$ T-cells, and also S-reactive CD4$^+$ and CD8$^+$ T-cells. In additional
209 experiments, we stained antigen-induced T-cells cells for the expression of interferon

210 gamma (IFNγ) and interleukin 4 (IL4). These experiments revealed that the S-reactive
211 $CD4^+$ T-cell population displayed elevated expression of the Th1-associated cytokine
212 IFNγ, and to a lesser extent, the Th2-associated cytokine IL4 (***Fig 7***). In contrast, N-
213 reactive T-cells failed to display an N-induced expression of either IFNγ or IL4.
214
215 ***Absence of vaccine-induced adverse reactions***
216 Control and vaccinated animals were examined regularly for overall appearance, general
217 behavior, and injection site inflammation (redness, swelling). No vaccine-related
218 differences were observed in any of these variables, and animals from all groups
219 displayed similar age-related increases in body mass (***supplemental figure 1***).
220 Vaccination also had no discernable effect on blood cell counts (***supplemental figure 2***).
221 Histological analyses were performed on all animals at the conclusion of the study by an
222 independent histology service, which reported that vaccinated animals showed no
223 difference in overall appearance of any of the tissues that were examined. Representative
224 images are presented for brain, lung, heart, liver, spleen, kidney, and side of injection
225 skeletal muscle in an animal from each of the trial groups (***Fig. 8***).
226
227

228 ***Discussion***

229 Exosomes are natural products of human cells that are more 'self' than 'non-self'. Immune
230 systems are tolerant of the high levels of exosomes that are continuously present in all
231 biofluids (e.g. blood, lymph, cerebrospinal fluid, vitreous, interstitial fluids, etc.) [49,58].
232 Furthermore, there is no evidence of adverse effects of allogeneic exosome transfer,
233 whether of purified exosomes (from amniotic fluid, blood, etc.) or of inadvertent exosome
234 transfer during tissue transplantation, blood transfusion, plasma injection, etc. In this
235 context, the fact that exosomes normally participate in pathways of vesicle-mediated,
236 intercellular RNA traffic [59-61] indicates that exosomes may be an ideal vehicle for clinical
237 RNA delivery. The data presented here support this hypothesis by showing that that
238 exosome-mRNA formulations can support the *in vivo*, functional expression of proteins
239 as diverse as soluble cytoplasmic enzymes, viral structural proteins, and synthetic fusion
240 proteins.

241

242 Our findings are also relevant to the ongoing battle against SARS-CoV-2. Current vaccine
243 strategies are all centered on inducing immunity to Spike, but Spike-only vaccines are
244 susceptible to escape effects whenever and antigenically shifted Spike variants starts to
245 spread in susceptible populations. While we are developing strategies designed to
246 address this challenge by improved design of expression-dependent Spike vaccines, we
247 are also working to address it by generating a multiplexed mRNA vaccine that delivers
248 two or more mRNAs, one encoding Spike and the others encoding Nucleocapsid and
249 perhaps fragments of other proteins as well. One limitation of this approach is that
250 Nucleocapsid is a cytoplasmic protein rather than a surface antigen, a topology that limits

251 its efficacy in vaccination studies. However, this limitation can be overcome by expressing
252 Nucleocapsid as part of a fusion with the lysosomal resident protein Lamp1, which places
253 Nucleocapsid protein in the correct compartments for Class I and Class II antigen
254 presentation (ER and lysosome/MHC Class II compartment, respectively). This approach
255 was realized in our LSNME/S^{W1} vaccine, which elicited strong cellular immune responses
256 to Nucleocapsid as well as to Spike. Vaccinated animals displayed antigen-induced $CD4^+$
257 and $CD8^+$ T-cell responses to both Nucleocapsid and to Spike that persisted for nearly
258 two months after immunization. Furthermore, when these cell populations were
259 interrogated for antigen-induced expression of the cytokines IFNγ and IL4, we detected
260 elevated expression of IFNγ in CD4+ T-cells exposed to exogenous Spike protein, as well
261 as a more modest Spike-induced expression of IL4. These results raise the possibility
262 that the exosome-based LSNME/S^{W1} vaccine induces the kind of Th1-skewed cellular
263 immune response desired for an anti-viral vaccine. Vaccinated animals also developed
264 durable antibody responses to the Nucleocapsid and the Spike proteins that were
265 sustained at relatively constant levels over the 7 weeks following immunization. This
266 multi-antigen immune response bodes well for this approach in the next generation of
267 SARS-CoV-2 vaccines that will be needed to protect against the emerging array of
268 antigenically distinct SARS-CoV-2 viral strains and their ever-increasing spectrum of
269 Spike protein mutations.
270
271 In conclusion, the results presented in this study validate the use of multiplexed exosome-
272 mRNA formulations for functional delivery of mRNAs both in cultured cells and in live
273 animals. The successful use of exosomes to deliver Antares2 mRNA opens the door to

274 follow-on studies aimed at optimizing exosome-RNA formulation conditions, as well as
275 for characterizing the time-dependence of Antares2 expression, biodistribution of
276 exosome-mediated RNA expression, injection site effects, and exosome-mediated tissue
277 tropism. As for the future development of exosome-based SARS-CoV-2 mRNA vaccines,
278 we anticipate that follow-on studies will demonstrate multiple advantages of exosome-
279 based delivery, improved antigen designed, and most importantly, improved protective
280 effects that arise from immunization with multiple viral antigens, and particularly
281 Nucleocapsid, which is a main target of anti-SARS-CoV-2 immunity in COVID-19 patients
282 [48] and has proven effective in vaccine studies of other coronaviruses [54]. Furthermore, the
283 fact that exosomes can be deployed at high concentrations without adverse effects on
284 cells or animals bodes well for their future use in dosing regimens that require higher-
285 level or ongoing repeated injections.
286
287

288 **Methods**

289

290 *Cell culture*

291 293F cells (Gibco, Cat.# 51-0029) were tested for pathogens and found to be free of viral
292 (cytomegalovirus, human immunodeficiency virus I and II, Epstein Barr virus, hepatitis B
293 virus, and parvovirus B19), and bacterial (*Mycoplasma*) contaminants. Cells were
294 maintained in FreeStyle 293 Expression Medium (Gibco, #12338-018) and incubated at
295 37°C in 8% CO_2. For exosome production, 293F cells were seeded at a density of 1.5 x
296 10^6 cells/ml in shaker flasks in a volume of ~1/4 the flask volume and grown at a shaking
297 speed of 110 rpm. HEK293 cells were grown in Dulbecco's modified Eagle's medium
298 supplemented with 10% fetal calf serum.

299

300 *Exosome purification*

301 293F cells were grown in shaker cultures for a period of three days. Cells and large cell
302 debris were removed by centrifugation at 300 x *g* for 5 minutes followed by 3000 x *g* for
303 15 minutes. The resulting supernatant was passed through a 0.22 µm sterile filtration filter
304 unit (Thermo Fisher, #566-0020) to generate a clarified tissue culture supernatant
305 (CTCS). The CTCS was concentrated by centrifugal filtration (Centricon Plus-70, Ultracel-
306 PL Membrane, 100 kDa size exclusion, Millipore Sigma # UFC710008), with ~120 mLs
307 CTCS concentrated to ~0.5 mLs. Concentrated CTCS was then purified by size exclusion
308 chromatography (SEC) in 1x PBS (qEV original columns/35 nm: Izon Science, #SP5),
309 with the exosomes present in each 0.5 mL starting sample eluting in three 0.5 mL
310 fractions. Purified exosomes were reconcentrated using Amicon® Ultra-4 100 kDa cutoff

311 spin columns (#UFC810024). This process yielded a population of exosomes/small EVs
312 that have the expected ultrastructure and size distribution profile of human exosomes and
313 contain the exosomal marker proteins CD9 and CD63 (***Fig. 8***), at a concentrating effect
314 of ~500-fold, to a final concentration of ~2 x 10^{12} exosomes/ml, representing an average
315 recovery of 35%.
316
317 *Nanoparticle Tracking Analysis (NTA)*
318 Vesicle concentrations and size distribution profiles of exosome preparations were
319 measured by nanoparticle tracking analysis (NTA) using a NanoSight NS300 (Malvern
320 Panalytical, United Kingdom) in 1x PBS clarified by filtration through a 0.22 µm sterile
321 filtration unit. Measurements were carried out in triplicates at ambient temperature with
322 fixed camera settings (level of 14, screen gain of 10, detection threshold 3, and
323 temperature of 21.7-22.2 °C). Immunostaining nanoparticle tracking analysis (NTA) was
324 performed using fluorescently labeled antibody conjugate directed against human CD63
325 (AlexaFluor488-conjugated clone 460305; R&D Systems (Minneapolis, USA)). The
326 fluorescently labeled anti-CD63-antibody (1 µl) was incubated with exosomes (9 µl) for 2
327 hours at room temperature in the dark, then diluted by addition of 1 ml of sterile-filtered
328 PBS (Thermo Fisher, USA) and examined for exosome abundance, size, and CD63
329 immunoreactivity using a Particle Metrix ZetaView® TWIN device. Samples were
330 visualized in scatter mode using the 488 nm laser and standard instrument settings
331 (sensitivity: 80, shutter: 100, min. brightness: 30; min. area: 10; max. area: 1000) in
332 fluorescence mode with standard fluorescence settings (sensitivity: 88, shutter: 100, min.

333 brightness: 25; min. area: 10; max. area: 1000). The resulting videos were analysed with
334 the ZetaView® software 8.05.10 (Particle Metrix, Germany).
335
336 *Immunoblots*
337 Exosome and cell lysates were separated by SDS-PAGE using pre-cast, 4-15% gradient
338 gels (Bio-Rad 4561086) and transferred to PVDF membranes (ThermoFisher, #88518).
339 Membranes were blocked, probed with antibodies directed against CD9 (clone HI9a;
340 BioLegend), CD63 (MX-49.129.5), CD81 (555675; BD Pharmingen), or HSP90 (sc-
341 13119; Santa Cruz Biotechnology), then washed, exposed to HRP-conjugates of goat
342 secondary antibodies (Jackson Immunoresearch), washed, and processed for
343 chemiluminescent imaging using HRP-activated chemiluminescence detection solution
344 (Amersham ECL Western Blotting Detection Reagents; cat# RPN2106), and imaged
345 using a GE Amersham Imager 600. Images were exported as JPEG files, analyzed using
346 ImageJ software, and processed using Photoshop (Adobe).
347
348 *Electron Microscopy and light microscopy*
349 Exosomes were fixed by addition of formaldehyde to a final concentration of 4%. Carbon-
350 coated grids were placed on top of a drop of the exosome suspension. Next, grids were
351 placed directly on top of a drop of 2% uranyl acetate. The resulting samples were
352 examined with a Tecnai-12 G2 Spirit Biotwin transmission electron microscope (John
353 Hopkins University, USA). Fluorescence micrographs of Antares2 expression in
354 transfected HEK293 cells were captured as PNG files using an EVOS M7000 microscope
355 equipped with an Olympus UPlanSAPo 40x/0.95 objective.

356

357 *Production of mRNA-loaded exosomes and LNPs*

358 mRNAs were obtained from a commercial provider (Trilink). mRNAs were purified using
359 RNeasy columns (Qiagen) and resuspended in DNase-free, RNase-free water using
360 nuclease-free tips and tubes. Purified mRNAs were pre-incubated with a coating of
361 polycationic lipids and then mixed with equal amounts of either purified exosomes or
362 LNPs (DOTAP/DOPE, #F50102, FormuMAx Scientific Inc) at 4°C for 10 minutes.
363 Formulations were either used immediately or frozen at -80°C and thawed rapidly prior to
364 use.

365

366 *Luciferase measurements and bioluminescent imaging*

367 HEK293 cells were incubated with exosome-mRNA formulations overnight under
368 standard culture conditions. Antares2 luciferase activity was measured by Live cell
369 bioluminescence was collected after incubating with substrate diphenylterazine (MCE,
370 HY-111382) at final concentration of 50 μM for 3 minutes. Readings were collected using
371 a SpectraMax i3x (Molecular Devices). For in vivo studies, thirteen months-old, female
372 Balb/c mice (Jackson Laboratory) housed under pathogen-free conditions at the Cedars-
373 Sinai Medical Center animal facility were used to study the expression of Exosome-
374 Anteres2 mRNA expression 24 hours after injection. Intramuscular injections were at a
375 volume of 50 μls per mouse containing 5 ug mRNA. After 24 hours the animals were
376 imaged using an IVIS Spectrum imager (PerkinElmer, Waltham, MA) (All animal
377 experimentation was performed following institutional guidelines for animal care and were
378 approved by the Cedars-Sinai Medical Center IACUC (#8602).

379

380 *Animal experimentation*

381 All animal experimentation was performed following institutional guidelines for animal
382 care and were approved by the Cedars-Sinai Medical Center IACUC (#8602). All
383 injections were at a volume of 50 μls. Experiments involved injection of exosomes, LNPS,
384 and Antares2 mRNA-loaded exosomes were performed with BALB/c mice (Jackson
385 Laboratory). Immunization with mRNA-loaded exosomes were performed on thirteen
386 weeks-old, male C57BL/6J mice (Jackson Laboratory) housed under pathogen-free
387 conditions at the Cedars-Sinai Medical Center animal facility. Blood (~0.1 mL) was
388 collected periodically from the orbital vein. At day 84, mice were deeply anesthetized
389 using isoflurane, euthanized by cervical dislocation, and processed using standard
390 surgical procedures to obtain spleen, lung, brain, heart, liver, kidney, muscle, and other
391 tissues. Spleens were processed for splenocyte analysis, and all tissues were processed
392 for histological analysis by fixation in 10% neutral buffered formalin. Histological analysis
393 was performed by the service arm of the HIC/Comparative Pathology Program of the
394 University of Washington.

395

396 *ELISA for SARS-CoV-2 antigen-specific antibody responses*

397 Mouse IgG antibody production against SARS-CoV-2 antigens was measured by
398 enzyme-linked immunosorbent assays (ELISA). For antigens S1 (RBD) and N, pre-
399 coated ELISA plates from RayBiotech were utilized (IEQ-CoV S RBD-IgG; IEQ-CoVN-
400 IgG), and the experiments were performed according to the manufacturer's instructions,
401 with modification. Briefly, mouse plasmas at dilutions of 1:50 were added to antigen pre-

402 coated wells in duplicates and incubated at room temperature (RT) for 2 hours on a
403 shaker (200 rpm). The plates were washed 4 times with wash buffer followed by blocking
404 for 2 hours at RT with 1% BSA in PBS. Mouse antibodies bound to the antigens coated
405 on the ELISA plates were detected using HRP-conjugated goat anti-mouse secondary
406 antibodies (Jackson Immuno Research Inc.) Plates were washed 4 times with washing
407 buffer, and developed using TMB substrate (RayBiotech). Microplate Reader was used
408 to measure the absorbance at 650 nm (SpectraMaxID3, Molecular Devices, with SoftMax
409 Pro7 software).
410
411 *Single cell splenocyte preparation*
412 After terminal blood collection, mice were euthanized, and part of fresh spleens were
413 harvested. Single cell splenocyte preparation was obtained by machinal passage through
414 a 40 µm nylon cell strainer (BD Falcon, #352340). Erythrocytes were depleted using
415 Ammonium-Chloride-Potassium (ACK) lysis buffer (Gibco, #A10492-01), and
416 splenocytes were washed using R10 media by centrifuging at 300x *g* for 5 minutes at RT.
417 R10 media (RPMI 1640 media (ATCC, Cat#302001) supplemented with 10% fetal bovine
418 serum (FBS) (Atlas, #E01C17A1), 50 µM 2-mercaptoethanol (Gibco, #21985-023),
419 penicillin/streptomycin (VWR life sciences, #K952), and 10 mM HEPES (Gibco, #15630-
420 080)) was used for all analyses of blood cells. The cells were resuspended in fresh media
421 and counted in hemocytometer counting chamber to be used in subsequent experiments.
422
423 *Spleen lymphocyte population characterization*

424 Splenocytes (2 x 10^5 cells/mouse) were resuspended in 100 µL of 10% FBS in 1x PBS
425 and incubated with fluorochrome-conjugated antibodies for surface staining of CD3
426 (Invitrogen, #17-0032-82) CD4 (Biolegend, #100433), CD8 (Biolegend, #100708), B220
427 (BD, #552771) CD11c (Invitrogen, #17-0114-81), F4/80 (Invitrogen, #MF48004) Ly6G
428 (Invitrogen, #11-9668-80) and Ly6C (BD, #560592)) for 30 minutes at 4 ˚C in the dark.
429 Following incubation, samples were washed twice with 200 µLs 10% FBS in 1x PBS and
430 centrifuged at 300 x *g* for 5 minutes at RT to remove unbound antibodies. Next the cells
431 were fixed with 100 µLs ICS fixation buffer (Invitrogen, #00-8222-49). Samples were
432 analyzed on a FACS Canto II (BD Biosciences) with 2,000 – 10,000 recorded
433 lymphocytes . The data analysis was performed using FlowJo 10 software (FlowJo, LLC)
434 and presented as a percentage change in the immune cell population compared to the
435 vehicle-treated group.
436
437 *SARS-CoV-2 antigen-specific T cell proliferation assay using CFSE*
438 Splenocytes were resuspended at 10^6 cells/mL in 10% FBS in 1xPBS and stained with
439 carboxyfluorescein succinimidyl ester (CFSE) (Invitrogen, #C34554) by rapidly mixing
440 equal volume of cell suspension with 10 µM CFSE in 10% FBS in 1x PBS for 5 minutes
441 at 37°C. The labeled cells were washed three times with R10 complete medium. The cells
442 were incubated for 96 hours in the presence of 10 µg/mL SARS-CoV-2 antigens N or S1
443 (Acro Biosystems, #NUN-C5227; SIN-C52H4) or medium alone as negative control. After
444 96 hours, cells were washed with 200 µLs 10% FBS in 1xPBS and centrifuged at 300 x *g*
445 for 5 minutes at RT. Cells were then stained with anti-CD3-APC (Invitrogen, #17-0032-
446 82), anti-CD4-PerCP-Cy5.5 (Biolegend, #100433), and anti-CD8-PE antibodies

447 (Biolegend, #MCD0801) for 30 minutes at 4˚C. The stained cells were washed twice with
448 200 µLs 1x PBS and analyzed on a FACS Canto II (BD Biosciences). For analysis,
449 lymphocytes were first gated for CD3+ T-cells, then for CD4+/CD8− or CD8+/CD4−
450 populations. The data analysis was performed using FlowJo 10 software (FlowJo LLC).
451
452 *Intracellular staining for cytokines*
453 2.0 x 10^5 splenocytes/mouse were incubated for 72 hours in the presence of 10 µg/mL
454 SARs-CoV2 antigens N or S1 (Acro Biosystems) or R10 medium alone (negative control).
455 After 72 hours, the cells were washed with fresh R10 medium and incubated with phorbol
456 myristate acetate (PMA) at concentration of 50 ng/mL (Sigma, #P1585), ionomycin at
457 concentration of 350 ng/mL (Invitrogen, #124222), and GogiPlug at concentration of 0.8
458 µL/mL (Invitrogen, #51-2301KZ) for 4 hours to amplify cytokine expression in T cells. The
459 cells were then washed with 10% FBS in 1x PBS and stained with anti-CD3-APC, anti-
460 CD4-PerCP-Cy5.5, and anti-CD8-PE antibodies (Added above) for 30 minutes at 4˚C in
461 dark. The cells were washed twice with 1xPBS followed by permeabilization step using
462 ready-to-use buffer (Invitrogen #00-8333-56). Next the cells were fixed with ICS fixation
463 bufferAdded above for 10 minutes at RT in dark and stained intracellular for IFN-γ
464 (eBioscience, #11-7311-82), IL-10 (eBioscience, #11-7101-82), IL-4 (Invitrogen, #12-
465 7041-41) and Foxp3 (Invitrogen, #12-5773-80) overnight at 4˚C in permeabilization buffer.
466 The stained cells were analyzed on a BD FACS Canto II with 5,000 – 10,000 recorded
467 lymphocytes. The data analysis was performed using FlowJo 10 software.
468
469 *Statistical Analysis*

470 Statistical analysis was performed using GraphPad Prism 8 software for Windows/Mac
471 (GraphPad Software, La Jolla California USA) or Excel. Results are reported as mean ±
472 standard deviation or mean ± standard error, and the differences were analyzed using
473 Student's t-test or one-way analysis of variance.
474
475

Sources of Support: This study was conducted with support from Capricor and from Johns Hopkins University.

Disclosures: S.J.G is a paid consultant for Capricor, holds equity in Capricor, and is co-inventor of intellectual property licensed by Capricor. S.J.T. is co-inventor of intellectual property licensed by Capricor. C.G. is co-inventor of intellectual property licensed by Capricor. A.S., S.K., J.N., S.S., C.L., and N.A. are employees of Capricor.

Acknowledgments: We thank Omid Sheikh for outstanding technical assistance during the course of these studies.

491 **Figure Legends**

492

493 *Figure 1. Exosome purification and characterization.* (A) Schematic of exosome
494 purification from cultures of 293F cells grown in chemically defined media. (B) NTA
495 analysis of purified exosomes showed a mean exosome diameter of ~115 nm. (C)
496 Negative stain electron micrograph of purified exosomes. Bar, 100 nm. (D)
497 Immunofluorescent NTA analysis of 293F-derived exosomes that had been labeled
498 previously using fluorescently labeled anti-CD63 antibody. (E) Immunoblot analysis of
499 equal proportions of 293F cell and exosome lysates using antibodies specific for the
500 exosomal markers CD81, CD9, & CD63, as well as the control cytoplasmic protein Hsp90.

501

502 *Figure 2. Exosomes display superior mRNA delivery characteristics*. Relative luciferase
503 activities (average +/- standard error of the mean) of cells treated with low or high
504 concentrations of mRNA-loaded exosomes or mRNA-loaded LNPs.

505

506 *Figure 3. Effect of exosome and LNP injections on organ histology and body* mass. (A)
507 H&E staining of tissue sections from BALB/c mice that had been injected three days
508 earlier with 50 ml of PBS, exosomes (10^{12}/ml), or LNPs (10^{12}/ml). (B) Body mass
509 measurements prior to and at 3 days after injection. All animals were subjected to analysis
510 by an independent pathology service, which noted spleen abnormalities in 4/5 LNP-
511 treated animals but no abnormalities in control or exosome-treated animals.

512

513 *Figure 4. Real-time imaging of exosome-mediated, functional mRNA delivery.* Combined
514 bioluminescent and light images of control mice and treated mice immediately following
515 i.p. administration of DTZ. Treated mice had been injected with Antares2 mRNA-loaded
516 exosomes 24 hours prior to imaging. Radiance is in photons/second/area
517 (cm^2)/steradian.
518
519 *Figure 5. Expression of S^{W1} and LSNME following mRNA transfection*. (A, B)
520 Fluorescence micrographs of HEK293 cells stained with DAPI and a plasma from a
521 COVID-19 patient. (C-F) Fluorescence micrographs of HEK293 cells stained with DAPI
522 and plasmas from a COVID-19 patient following their transfection with the (C, D) S^{W1}-
523 encoding mRNA and (E, F) the LSNME-encoding mRNA. Bar, 50 µm.
524
525 *Figure 6. LSNME/S^{W1} vaccination induces antibody responses to SARS-CoV-2 N and S*
526 *protein*. (A) Schematic of immunization and blood/tissue collection timeline. (B) Anti-N
527 ELISA results of diluted plasma from (grey bars and black circles) individual six control
528 mice, (orange bars and black squares) six mice immunized with 0.25 µg equivalents of
529 each mRNA, and (rust bars and black triangles) six mice immunized with 4 µg equivalents
530 of each mRNA. (C) Anti-S1 ELISA results of diluted plasma from (grey bars and black
531 circles) individual six control mice, (orange bars and black squares) six mice immunized
532 with 0.25 µg equivalents of each mRNA, and (rust bars and black triangles) six mice
533 immunized with 4 µg equivalents of each mRNA. Height of bars represents the mean,
534 error bars represent +/- one standard error of the mean, and the statistical significance of

535 differences between different groups is reflected in Student's t-test values of * for <0.05,
536 ** for <0.005, and *** for <0.0005.
537
538 *Figure 7. LSNME/S^{W1} vaccination induces $CD4^+$ and $CD8^+$ T-cell responses*. CFSE-
539 labeled splenocytes were interrogated by flow cytometry following incubation in the
540 absence or presence of (A, B) purified, recombinant N protein or (C, D) purified,
541 recombinant S protein, and for antibodies specific for CD4 and CD8. Differences in
542 proliferation of $CD4^+$ cells and $CD8^+$ cells were plotted for (grey bars and black circles)
543 individual six control mice, (orange bars and black squares) six mice immunized with 0.25
544 μg equivalents of each mRNA, and (rust bars and black triangles) six mice immunized
545 with 4 μg equivalents of each mRNA. Height of bars represents the mean, error bars
546 represent +/- one standard error of the mean, and the statistical significance of differences
547 between different groups is reflected in Student's t-test values of * for <0.05 and ** for
548 <0.005.
549
550 *Figure 8. LSNME/S^{W1} vaccination leads to S-induced expression of IFNγ and IL4 by $CD4^+$*
551 *T-cells*. Splenocytes were interrogated by flow cytometry following incubation in the
552 absence or presence of (A, B) purified, recombinant N protein or (C, D) purified,
553 recombinant S protein, and labeling with antibodies specific for CD4 or CD8, and for IFNγ
554 or IL4. Differences in labeling for IFNγ or IL4 in $CD4^+$ $CD8^+$ cell populations were plotted
555 for (grey bars and black circles) individual six control mice, (orange bars and black
556 squares) six mice immunized with 0.25 μg equivalents of each mRNA, and (rust bars and
557 black triangles) six mice immunized with 4 μg equivalents of each mRNA. Height of bars

558 represents the mean, error bars represent +/- one standard error of the mean, and the
559 statistical significance of differences between different groups is reflected in Student's t-
560 test values of * for <0.05.
561
562 *Figure 9. Absence of tissue pathology upon LSNME/S^{W1} vaccination.* Representative
563 micrographs from histological analysis (hematoxylin and eosin stain) of lung, brain, heart,
564 liver, kidney, spleen, and muscle (side of injection) of animals from (upper row) control
565 mice, (middle row) mice immunized with the lower dose of the LSNME/S^{W1} vaccine, and
566 (lower row) mice immunized with the higher dose of the LSNME/S^{W1} vaccine.
567
568
569
570
571

572 *Supplemental Figure 1. Equivalent growth of vaccinated and control animals*. Body mass
573 of all mice was measured over the course of the study and plotted as average +/- the
574 standard error of the mean, relative to the body mass at the initiation of the trial, with
575 groups reported as (grey lines and circles) control mice, (orange lines and squares) lower
576 dose-treated mice, and (rust lines and triangles) higher dose-treated mice.
577
578 *Supplemental Figure 2. Vaccination does not induce changes in the proportional*
579 *representation of key blood cell populations*. Splenocytes were interrogated by flow
580 cytometry using antibodies specific for (A) B220, (B) Ly6C, (C) CD11c, and (D) CD3.
581 $CD3^+$ cells were further differentiated by staining for (E) CD4 and (F) CD8. No statistically
582 significant differences were detected in these subpopulations of white blood cells.
583
584
585

586

587 ## References

588 1 Zhou, P. *et al.* A pneumonia outbreak associated with a new coronavirus of probable bat
589 origin. *Nature* **579**, 270-273, doi:10.1038/s41586-020-2012-7 (2020).
590 2 Coronaviridae Study Group of the International Committee on Taxonomy of, V. The
591 species Severe acute respiratory syndrome-related coronavirus: classifying 2019-nCoV
592 and naming it SARS-CoV-2. *Nat Microbiol* **5**, 536-544, doi:10.1038/s41564-020-0695-z
593 (2020).
594 3 Gandhi, R. T., Lynch, J. B. & Del Rio, C. Mild or Moderate Covid-19. *N Engl J Med* **383**, 1757-
595 1766, doi:10.1056/NEJMcp2009249 (2020).
596 4 Wang, D. *et al.* Clinical Characteristics of 138 Hospitalized Patients With 2019 Novel
597 Coronavirus-Infected Pneumonia in Wuhan, China. *JAMA* **323**, 1061-1069,
598 doi:10.1001/jama.2020.1585 (2020).
599 5 Zhou, F. *et al.* Clinical course and risk factors for mortality of adult inpatients with COVID-
600 19 in Wuhan, China: a retrospective cohort study. *Lancet* **395**, 1054-1062,
601 doi:10.1016/S0140-6736(20)30566-3 (2020).
602 6 Force, A. D. T. *et al.* Acute respiratory distress syndrome: the Berlin Definition. *JAMA* **307**,
603 2526-2533, doi:10.1001/jama.2012.5669 (2012).
604 7 Richardson, S. *et al.* Presenting Characteristics, Comorbidities, and Outcomes Among
605 5700 Patients Hospitalized With COVID-19 in the New York City Area. *JAMA* **323**, 2052-
606 2059, doi:10.1001/jama.2020.6775 (2020).
607 8 Guo, T. *et al.* Cardiovascular Implications of Fatal Outcomes of Patients With Coronavirus
608 Disease 2019 (COVID-19). *JAMA Cardiol* **5**, 811-818, doi:10.1001/jamacardio.2020.1017
609 (2020).
610 9 Boni, M. F. *et al.* Evolutionary origins of the SARS-CoV-2 sarbecovirus lineage responsible
611 for the COVID-19 pandemic. *Nat Microbiol* **5**, 1408-1417, doi:10.1038/s41564-020-0771-
612 4 (2020).
613 10 Graham, R. L. & Baric, R. S. Recombination, reservoirs, and the modular spike:
614 mechanisms of coronavirus cross-species transmission. *J Virol* **84**, 3134-3146,
615 doi:10.1128/JVI.01394-09 (2010).
616 11 Corman, V. M., Muth, D., Niemeyer, D. & Drosten, C. Hosts and Sources of Endemic
617 Human Coronaviruses. *Adv Virus Res* **100**, 163-188, doi:10.1016/bs.aivir.2018.01.001
618 (2018).
619 12 Korber, B. *et al.* Tracking Changes in SARS-CoV-2 Spike: Evidence that D614G Increases
620 Infectivity of the COVID-19 Virus. *Cell* **182**, 812-827 e819, doi:10.1016/j.cell.2020.06.043
621 (2020).
622 13 Alam, I. *et al.* CovMT: an interactive SARS-CoV-2 mutation tracker, with a focus on critical
623 variants. *Lancet Infect Dis*, doi:10.1016/S1473-3099(21)00078-5 (2021).
624 14 Ho, D. *et al.* Increased Resistance of SARS-CoV-2 Variants B.1.351 and B.1.1.7 to Antibody
625 Neutralization. *Res Sq*, doi:10.21203/rs.3.rs-155394/v1 (2021).

15 Diamond, M. *et al.* SARS-CoV-2 variants show resistance to neutralization by many monoclonal and serum-derived polyclonal antibodies. *Res Sq*, doi:10.21203/rs.3.rs-228079/v1 (2021).
16 Hoffmann, M. *et al.* SARS-CoV-2 Cell Entry Depends on ACE2 and TMPRSS2 and Is Blocked by a Clinically Proven Protease Inhibitor. *Cell* **181**, 271-280 e278, doi:10.1016/j.cell.2020.02.052 (2020).
17 Matheson, N. J. & Lehner, P. J. How does SARS-CoV-2 cause COVID-19? *Science* **369**, 510-511, doi:10.1126/science.abc6156 (2020).
18 Daly, J. L. *et al.* Neuropilin-1 is a host factor for SARS-CoV-2 infection. *Science*, doi:10.1126/science.abd3072 (2020).
19 Cantuti-Castelvetri, L. *et al.* Neuropilin-1 facilitates SARS-CoV-2 cell entry and infectivity. *Science*, doi:10.1126/science.abd2985 (2020).
20 Wang, K. *et al.* CD147-spike protein is a novel route for SARS-CoV-2 infection to host cells. *Signal Transduct Target Ther* **5**, 283, doi:10.1038/s41392-020-00426-x (2020).
21 Wei, J. *et al.* Genome-wide CRISPR Screens Reveal Host Factors Critical for SARS-CoV-2 Infection. *Cell* **184**, 76-91 e13, doi:10.1016/j.cell.2020.10.028 (2021).
22 Mason, R. J. Thoughts on the alveolar phase of COVID-19. *Am J Physiol Lung Cell Mol Physiol* **319**, L115-L120, doi:10.1152/ajplung.00126.2020 (2020).
23 Nicin, L. *et al.* Cell type-specific expression of the putative SARS-CoV-2 receptor ACE2 in human hearts. *Eur Heart J* **41**, 1804-1806, doi:10.1093/eurheartj/ehaa311 (2020).
24 Li, M. Y., Li, L., Zhang, Y. & Wang, X. S. Expression of the SARS-CoV-2 cell receptor gene ACE2 in a wide variety of human tissues. *Infect Dis Poverty* **9**, 45, doi:10.1186/s40249-020-00662-x (2020).
25 Ziegler, C. G. K. *et al.* SARS-CoV-2 Receptor ACE2 Is an Interferon-Stimulated Gene in Human Airway Epithelial Cells and Is Detected in Specific Cell Subsets across Tissues. *Cell* **181**, 1016-1035 e1019, doi:10.1016/j.cell.2020.04.035 (2020).
26 Singh, M., Bansal, V. & Feschotte, C. A Single-Cell RNA Expression Map of Human Coronavirus Entry Factors. *Cell Rep* **32**, 108175, doi:10.1016/j.celrep.2020.108175 (2020).
27 V'Kovski, P., Kratzel, A., Steiner, S., Stalder, H. & Thiel, V. Coronavirus biology and replication: implications for SARS-CoV-2. *Nat Rev Microbiol*, doi:10.1038/s41579-020-00468-6 (2020).
28 Ujike, M. & Taguchi, F. Incorporation of spike and membrane glycoproteins into coronavirus virions. *Viruses* **7**, 1700-1725, doi:10.3390/v7041700 (2015).
29 Ruch, T. R. & Machamer, C. E. The coronavirus E protein: assembly and beyond. *Viruses* **4**, 363-382, doi:10.3390/v4030363 (2012).
30 Yao, H. *et al.* Molecular Architecture of the SARS-CoV-2 Virus. *Cell* **183**, 730-738 e713, doi:10.1016/j.cell.2020.09.018 (2020).
31 Hoffmann, M., Kleine-Weber, H. & Pohlmann, S. A Multibasic Cleavage Site in the Spike Protein of SARS-CoV-2 Is Essential for Infection of Human Lung Cells. *Mol Cell* **78**, 779-784 e775, doi:10.1016/j.molcel.2020.04.022 (2020).
32 Walls, A. C. *et al.* Structure, Function, and Antigenicity of the SARS-CoV-2 Spike Glycoprotein. *Cell* **181**, 281-292 e286, doi:10.1016/j.cell.2020.02.058 (2020).
33 Deng, W. *et al.* Primary exposure to SARS-CoV-2 protects against reinfection in rhesus macaques. *Science* **369**, 818-823, doi:10.1126/science.abc5343 (2020).

670 34 Chandrashekar, A. *et al.* SARS-CoV-2 infection protects against rechallenge in rhesus
671 macaques. *Science* **369**, 812-817, doi:10.1126/science.abc4776 (2020).
672 35 Shan, C. *et al.* Infection with novel coronavirus (SARS-CoV-2) causes pneumonia in Rhesus
673 macaques. *Cell Res* **30**, 670-677, doi:10.1038/s41422-020-0364-z (2020).
674 36 Bosco-Lauth, A. M. *et al.* Experimental infection of domestic dogs and cats with SARS-CoV-
675 2: Pathogenesis, transmission, and response to reexposure in cats. *Proc Natl Acad Sci U S*
676 *A* **117**, 26382-26388, doi:10.1073/pnas.2013102117 (2020).
677 37 St John, A. L. & Rathore, A. P. S. Early Insights into Immune Responses during COVID-19. *J*
678 *Immunol* **205**, 555-564, doi:10.4049/jimmunol.2000526 (2020).
679 38 Poland, G. A., Ovsyannikova, I. G. & Kennedy, R. B. SARS-CoV-2 immunity: review and
680 applications to phase 3 vaccine candidates. *Lancet*, doi:10.1016/S0140-6736(20)32137-1
681 (2020).
682 39 Zost, S. J. *et al.* Potently neutralizing and protective human antibodies against SARS-CoV-
683 2. *Nature* **584**, 443-449, doi:10.1038/s41586-020-2548-6 (2020).
684 40 Tizard, I. R. Vaccination against coronaviruses in domestic animals. *Vaccine* **38**, 5123-
685 5130, doi:10.1016/j.vaccine.2020.06.026 (2020).
686 41 Walsh, E. E. *et al.* Safety and Immunogenicity of Two RNA-Based Covid-19 Vaccine
687 Candidates. *N Engl J Med*, doi:10.1056/NEJMoa2027906 (2020).
688 42 Keech, C. *et al.* Phase 1-2 Trial of a SARS-CoV-2 Recombinant Spike Protein Nanoparticle
689 Vaccine. *N Engl J Med*, doi:10.1056/NEJMoa2026920 (2020).
690 43 Jackson, L. A. *et al.* An mRNA Vaccine against SARS-CoV-2 - Preliminary Report. *N Engl J*
691 *Med*, doi:10.1056/NEJMoa2022483 (2020).
692 44 Hassan, A. O. *et al.* A Single-Dose Intranasal ChAd Vaccine Protects Upper and Lower
693 Respiratory Tracts against SARS-CoV-2. *Cell* **183**, 169-184 e113,
694 doi:10.1016/j.cell.2020.08.026 (2020).
695 45 Zhu, F. C. *et al.* Immunogenicity and safety of a recombinant adenovirus type-5-vectored
696 COVID-19 vaccine in healthy adults aged 18 years or older: a randomised, double-blind,
697 placebo-controlled, phase 2 trial. *Lancet* **396**, 479-488, doi:10.1016/S0140-
698 6736(20)31605-6 (2020).
699 46 Bos, R. *et al.* Ad26 vector-based COVID-19 vaccine encoding a prefusion-stabilized SARS-
700 CoV-2 Spike immunogen induces potent humoral and cellular immune responses. *NPJ*
701 *Vaccines* **5**, 91, doi:10.1038/s41541-020-00243-x (2020).
702 47 Graham, S. P. *et al.* Evaluation of the immunogenicity of prime-boost vaccination with the
703 replication-deficient viral vectored COVID-19 vaccine candidate ChAdOx1 nCoV-19. *NPJ*
704 *Vaccines* **5**, 69, doi:10.1038/s41541-020-00221-3 (2020).
705 48 Burbelo, P. D. *et al.* Sensitivity in Detection of Antibodies to Nucleocapsid and Spike
706 Proteins of Severe Acute Respiratory Syndrome Coronavirus 2 in Patients With
707 Coronavirus Disease 2019. *J Infect Dis* **222**, 206-213, doi:10.1093/infdis/jiaa273 (2020).
708 49 Pegtel, D. M. & Gould, S. J. Exosomes. *Annu Rev Biochem* **88**, 487-514,
709 doi:10.1146/annurev-biochem-013118-111902 (2019).
710 50 Kamerkar, S. *et al.* Exosomes facilitate therapeutic targeting of oncogenic KRAS in
711 pancreatic cancer. *Nature* **546**, 498-503, doi:10.1038/nature22341 (2017).

712 51 Li, L. *et al.* Extracellular vesicles carry microRNA-195 to intrahepatic cholangiocarcinoma
713 and improve survival in a rat model. *Hepatology* **65**, 501-514, doi:10.1002/hep.28735
714 (2017).
715 52 Hassett, K. J. *et al.* Optimization of Lipid Nanoparticles for Intramuscular Administration
716 of mRNA Vaccines. *Mol Ther Nucleic Acids* **15**, 1-11, doi:10.1016/j.omtn.2019.01.013
717 (2019).
718 53 Yeh, H. W. *et al.* Red-shifted luciferase-luciferin pairs for enhanced bioluminescence
719 imaging. *Nat Methods* **14**, 971-974, doi:10.1038/nmeth.4400 (2017).
720 54 Gupta, V. *et al.* SARS coronavirus nucleocapsid immunodominant T-cell epitope cluster is
721 common to both exogenous recombinant and endogenous DNA-encoded immunogens.
722 *Virology* **347**, 127-139, doi:10.1016/j.virol.2005.11.042 (2006).
723 55 Vyas, J. M., Van der Veen, A. G. & Ploegh, H. L. The known unknowns of antigen processing
724 and presentation. *Nat Rev Immunol* **8**, 607-618, doi:10.1038/nri2368 (2008).
725 56 Imai, J., Otani, M. & Sakai, T. Distinct Subcellular Compartments of Dendritic Cells Used
726 for Cross-Presentation. *Int J Mol Sci* **20**, doi:10.3390/ijms20225606 (2019).
727 57 Guo, C. *et al.* The D614G Mutation Enhances the Lysosomal Trafficking of SARS-CoV-2
728 Spike. *bioRxiv*, doi:10.1101/2020.12.08.417022 (2020).
729 58 Yu, W. *et al.* Exosome-based Liquid Biopsies in Cancer: Opportunities and Challenges. *Ann*
730 *Oncol*, doi:10.1016/j.annonc.2021.01.074 (2021).
731 59 Skog, J. *et al.* Glioblastoma microvesicles transport RNA and proteins that promote
732 tumour growth and provide diagnostic biomarkers. *Nat Cell Biol* **10**, 1470-1476,
733 doi:10.1038/ncb1800 (2008).
734 60 Ratajczak, J. *et al.* Embryonic stem cell-derived microvesicles reprogram hematopoietic
735 progenitors: evidence for horizontal transfer of mRNA and protein delivery. *Leukemia* **20**,
736 847-856, doi:10.1038/sj.leu.2404132 (2006).
737 61 O'Brien, K., Breyne, K., Ughetto, S., Laurent, L. C. & Breakefield, X. O. RNA delivery by
738 extracellular vesicles in mammalian cells and its applications. *Nat Rev Mol Cell Biol* **21**,
739 585-606, doi:10.1038/s41580-020-0251-y (2020).
740

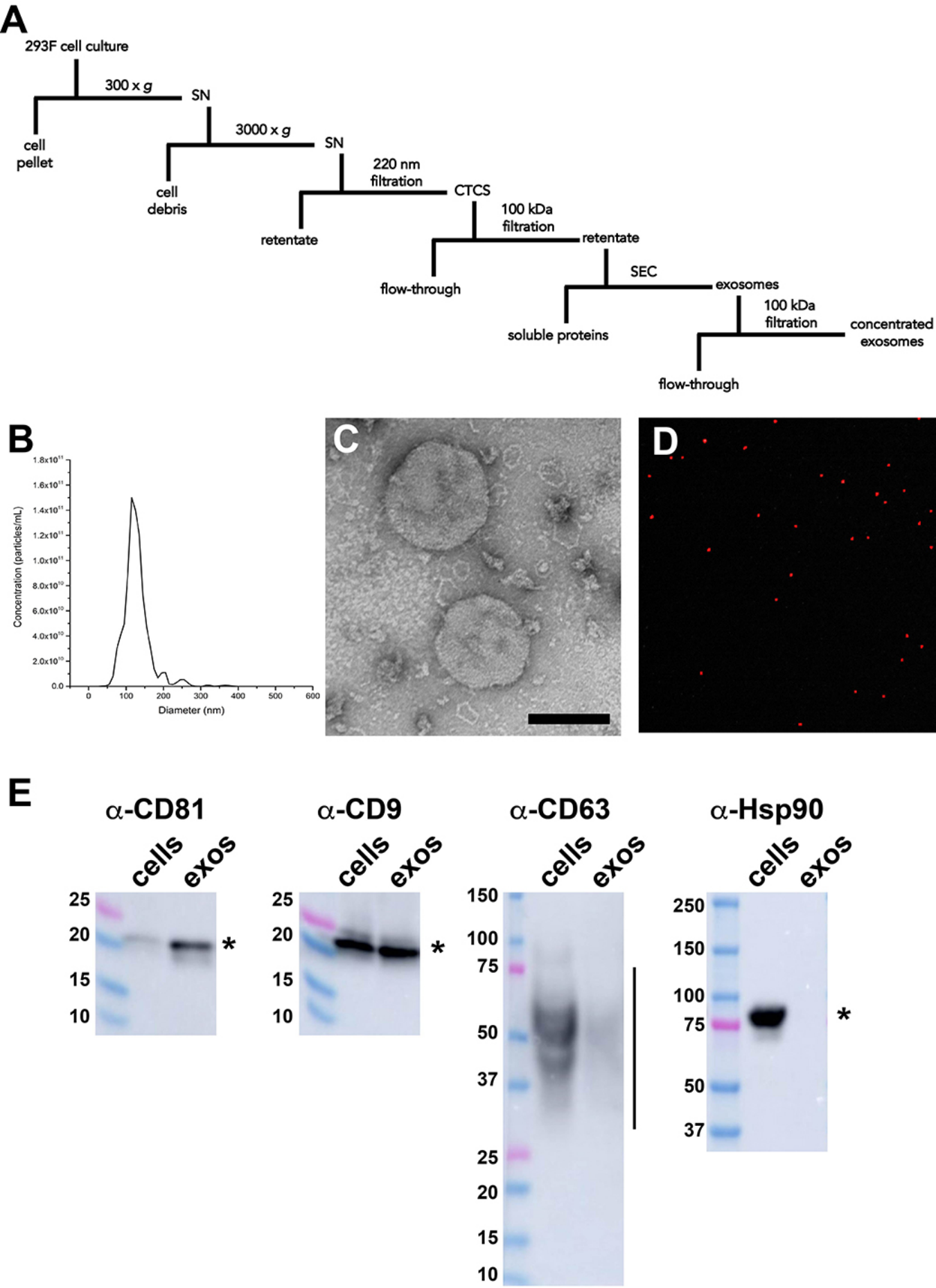
A
293F cell culture
300 x g
SN
cell pellet
3000 x g
SN
cell debris
220 nm filtration
CTCS
retentate
100 kDa filtration
retentate
flow-through
SEC
exosomes
soluble proteins
100 kDa filtration
concentrated exosomes
flow-through
B
Concentration (particles/mL)
Diameter (nm)
C
D
E
α-CD81
α-CD9
α-CD63
α-Hsp90
cells
exos
25
20
15
10
150
100
75
50
37
250
*

Figure 1

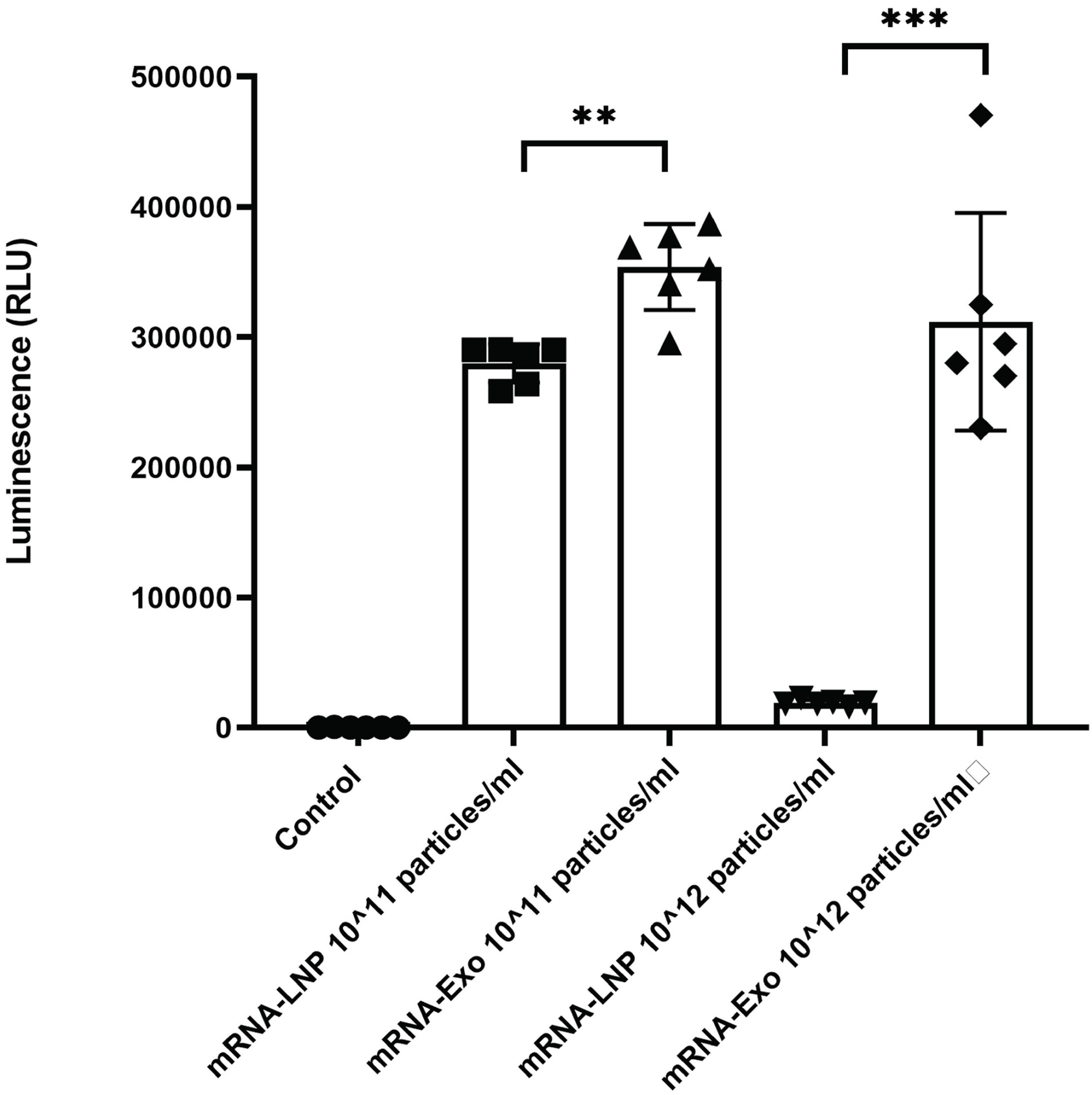
***
**
500000
400000
300000
200000
100000
0
Luminescence (RLU)
Control
mRNA-LNP 10^11 particles/ml
mRNA-Exo 10^11 particles/ml
mRNA-LNP 10^12 particles/ml
mRNA-Exo 10^12 particles/ml

Figure 2

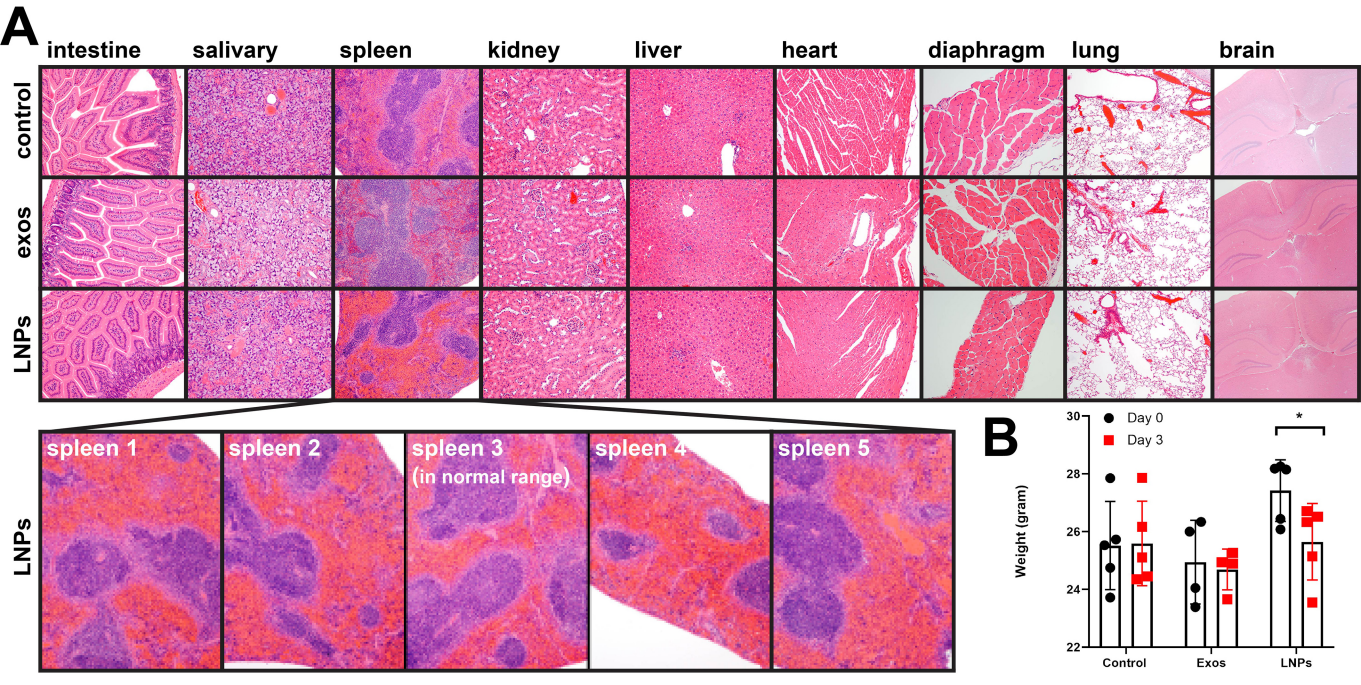
A
intestine
salivary
spleen
kidney
liver
heart
diaphragm
lung
brain
control
exos
LNPs
LNPs
spleen 1
spleen 2
spleen 3
(in normal range)
spleen 4
spleen 5
B
Day 0
Day 3
Weight (gram)
30
28
26
24
22
*
Control
Exos
LNPs

Figure 3

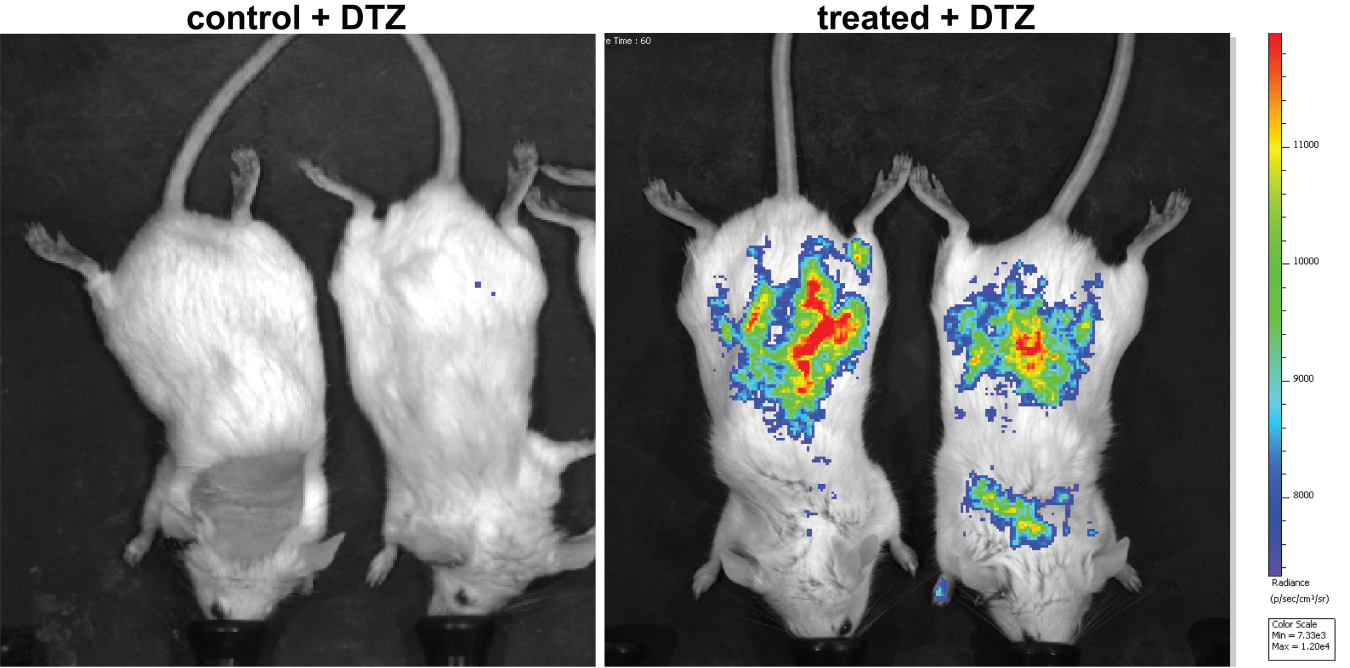
control + DTZ
treated + DTZ
e Time : 60
11000
10000
9000
8000
Radiance
(p/sec/cm²/sr)
Color Scale
Min = 7.33e3
Max = 1.20e4

Figure 4

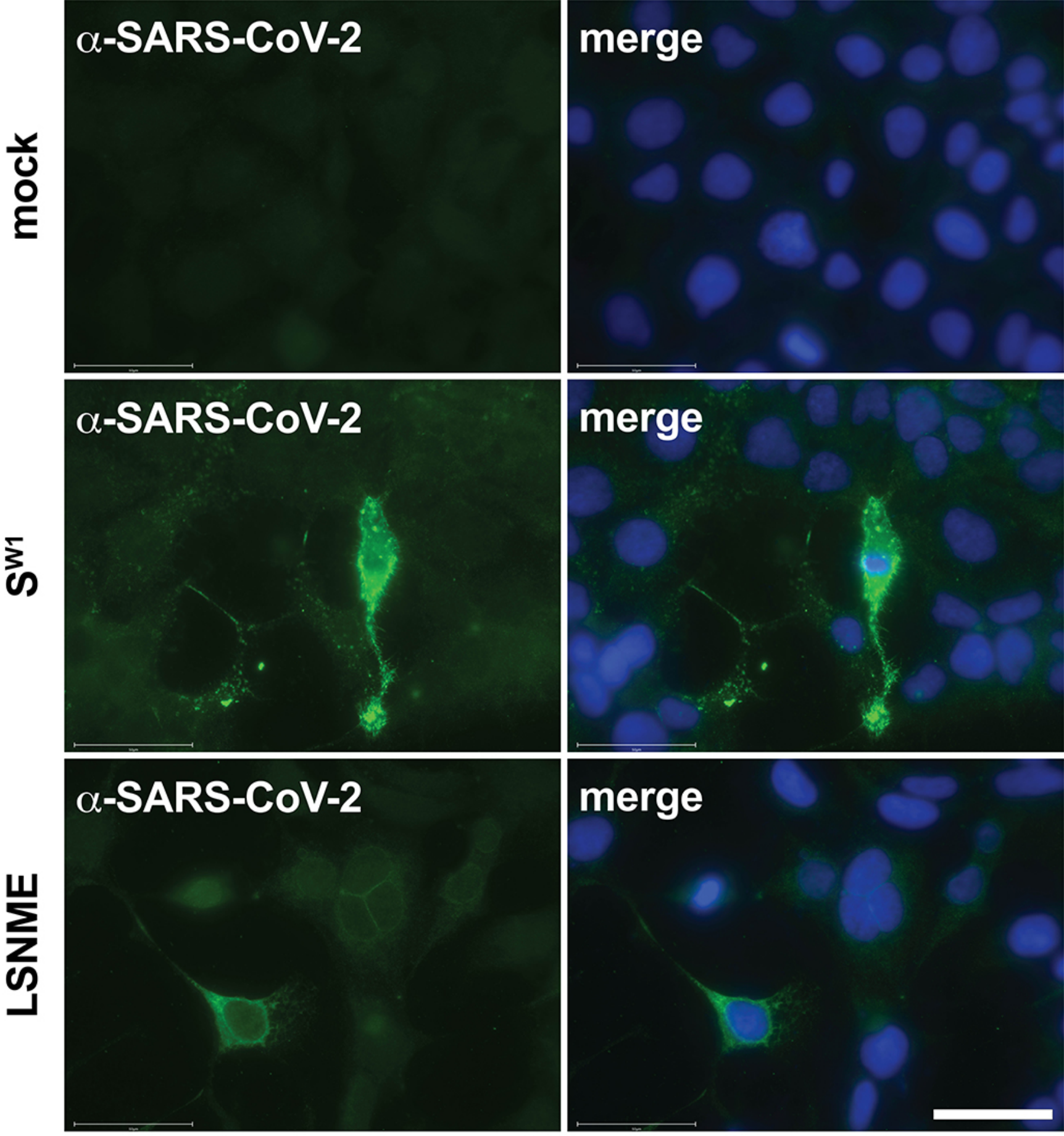
α-SARS-CoV-2
merge
mock
α-SARS-CoV-2
merge
SW1
α-SARS-CoV-2
merge
LSNME

Figure 5

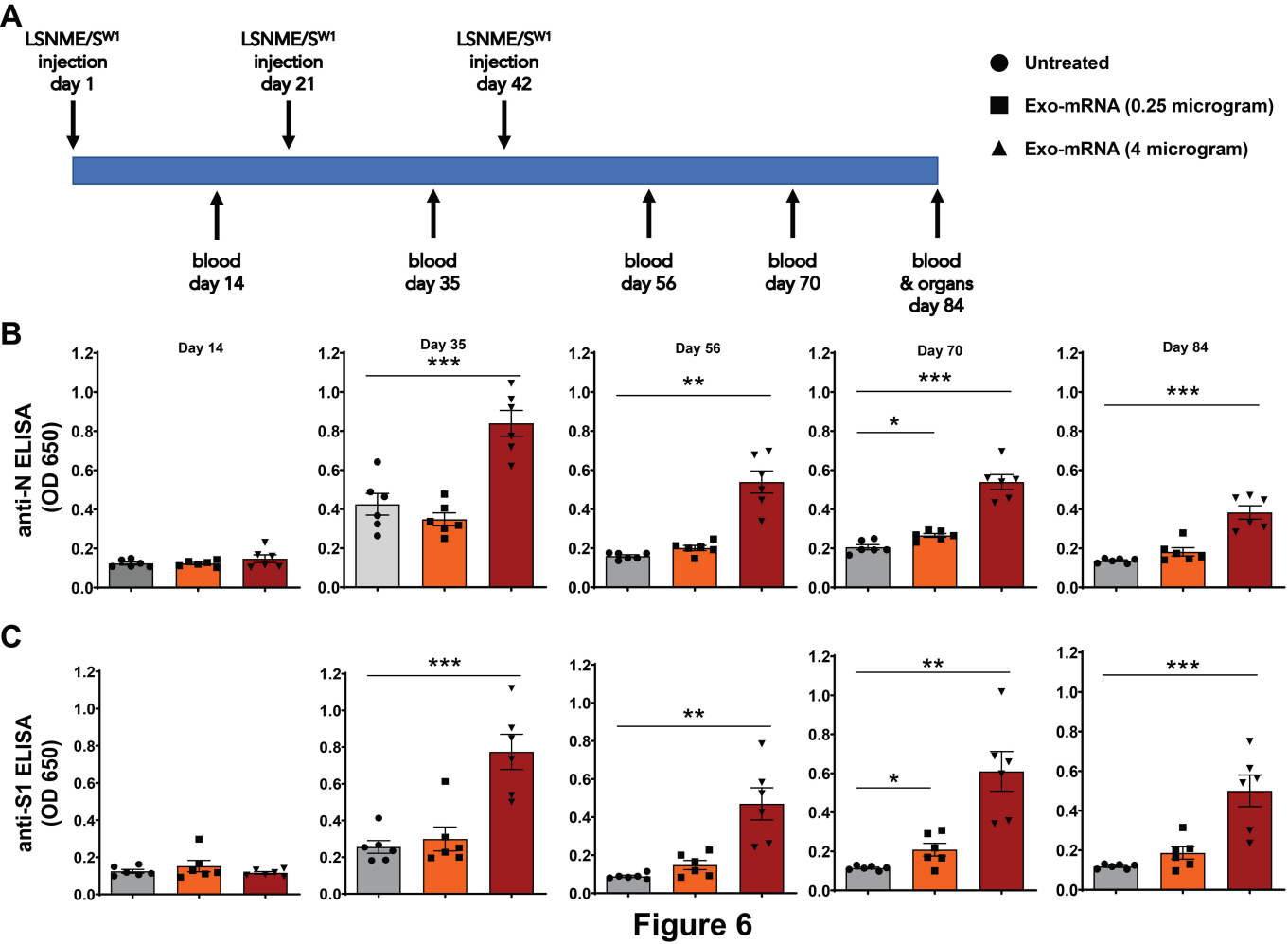
A
LSNME/SW1 injection day 1
LSNME/SW1 injection day 21
LSNME/SW1 injection day 42
Untreated
Exo-mRNA (0.25 microgram)
Exo-mRNA (4 microgram)
blood day 14
blood day 35
blood day 56
blood day 70
blood & organs day 84
B
anti-N ELISA (OD 650)
Day 14
Day 35
Day 56
Day 70
Day 84
C
anti-S1 ELISA (OD 650)

Figure 6

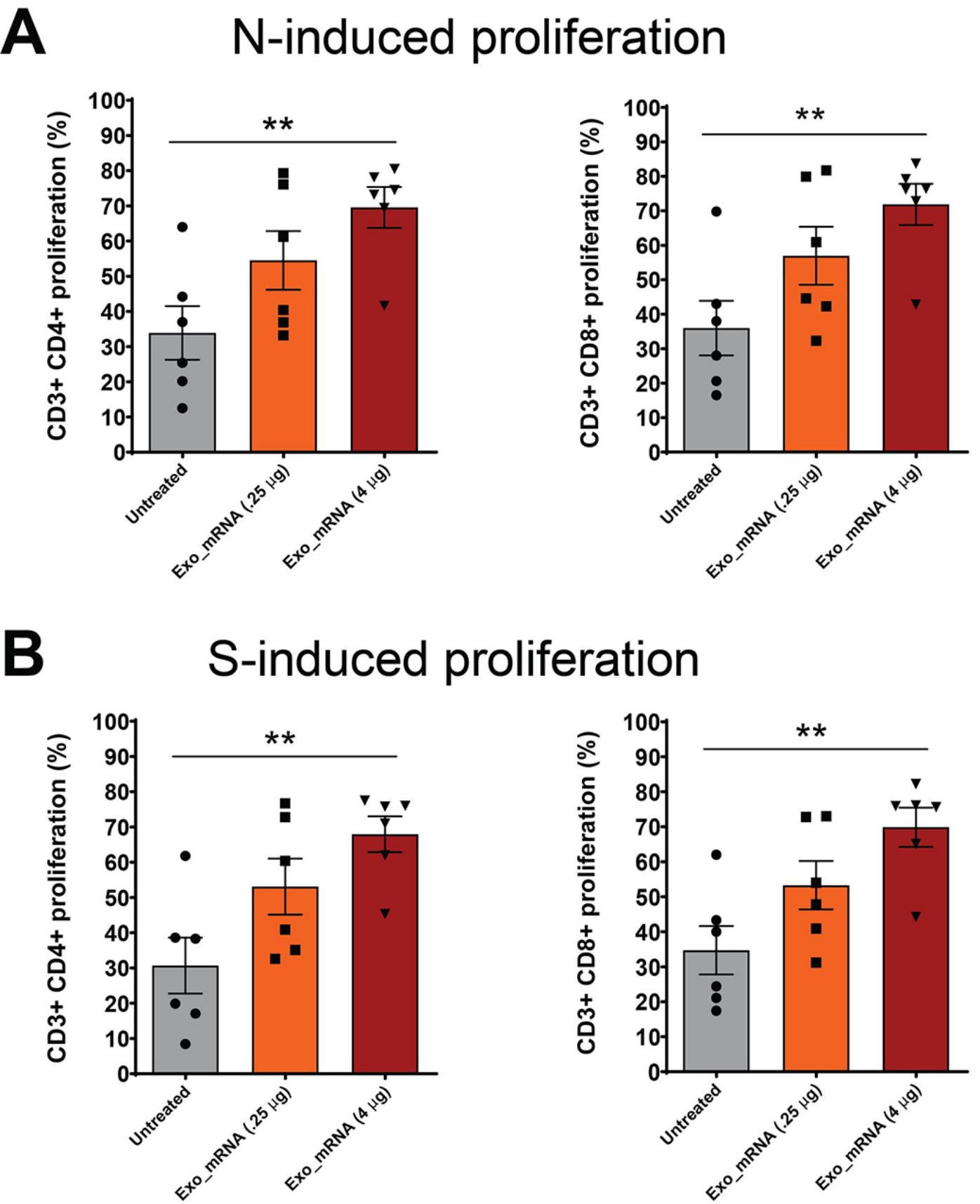
A
N-induced proliferation
CD3+ CD4+ proliferation (%)
CD3+ CD8+ proliferation (%)
**
Untreated
Exo_mRNA (.25 µg)
Exo_mRNA (4 µg)
B
S-induced proliferation
CD3+ CD4+ proliferation (%)
CD3+ CD8+ proliferation (%)
**
Untreated
Exo_mRNA (.25 µg)
Exo_mRNA (4 µg)

Figure 7

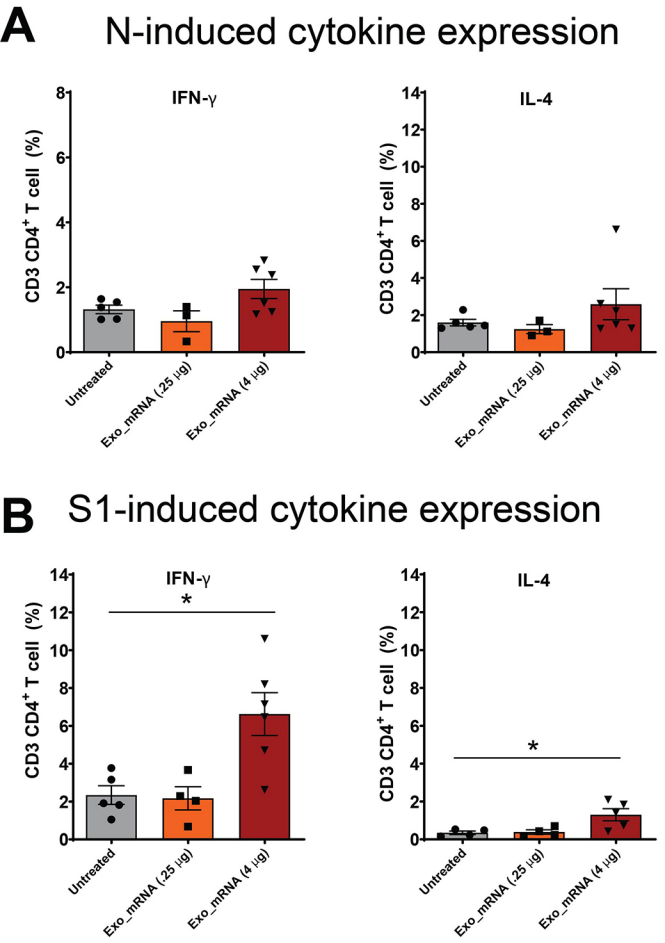
A
N-induced cytokine expression
IFN-γ
IL-4
CD3 CD4+ T cell (%)
Untreated
Exo_mRNA (.25 µg)
Exo_mRNA (4 µg)
B
S1-induced cytokine expression
IFN-γ
IL-4
*
*

Figure 8

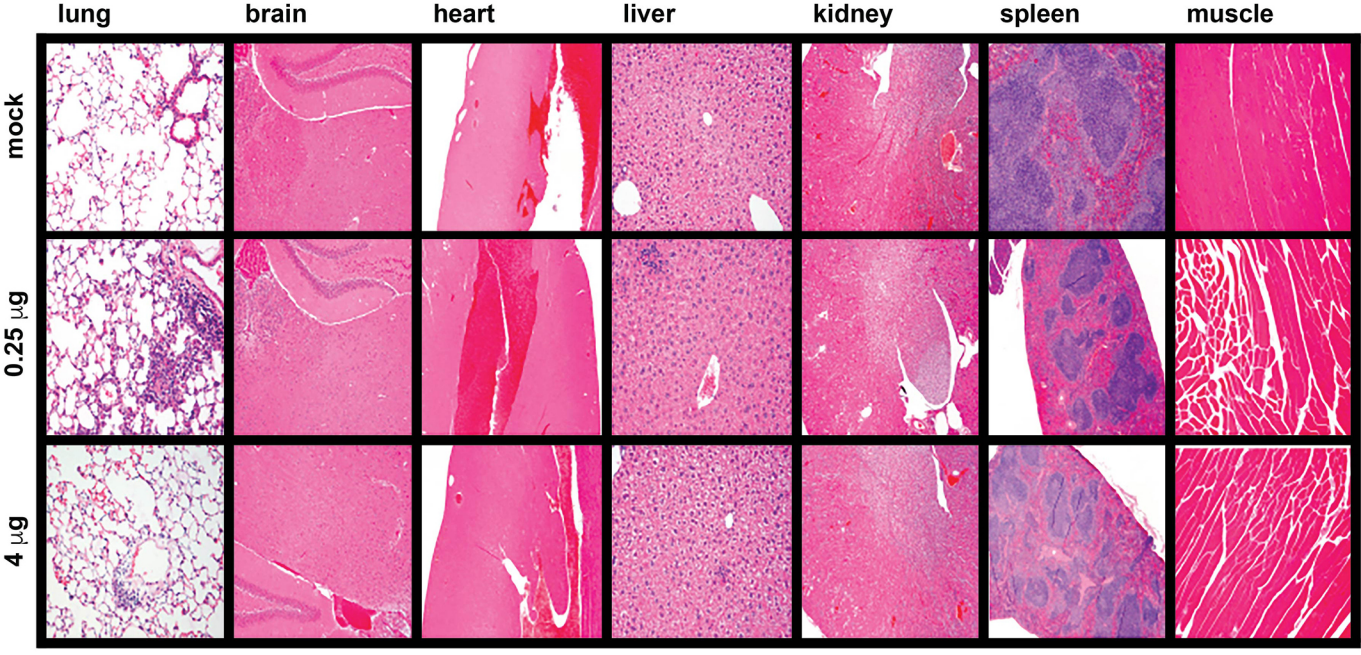

Figure 9

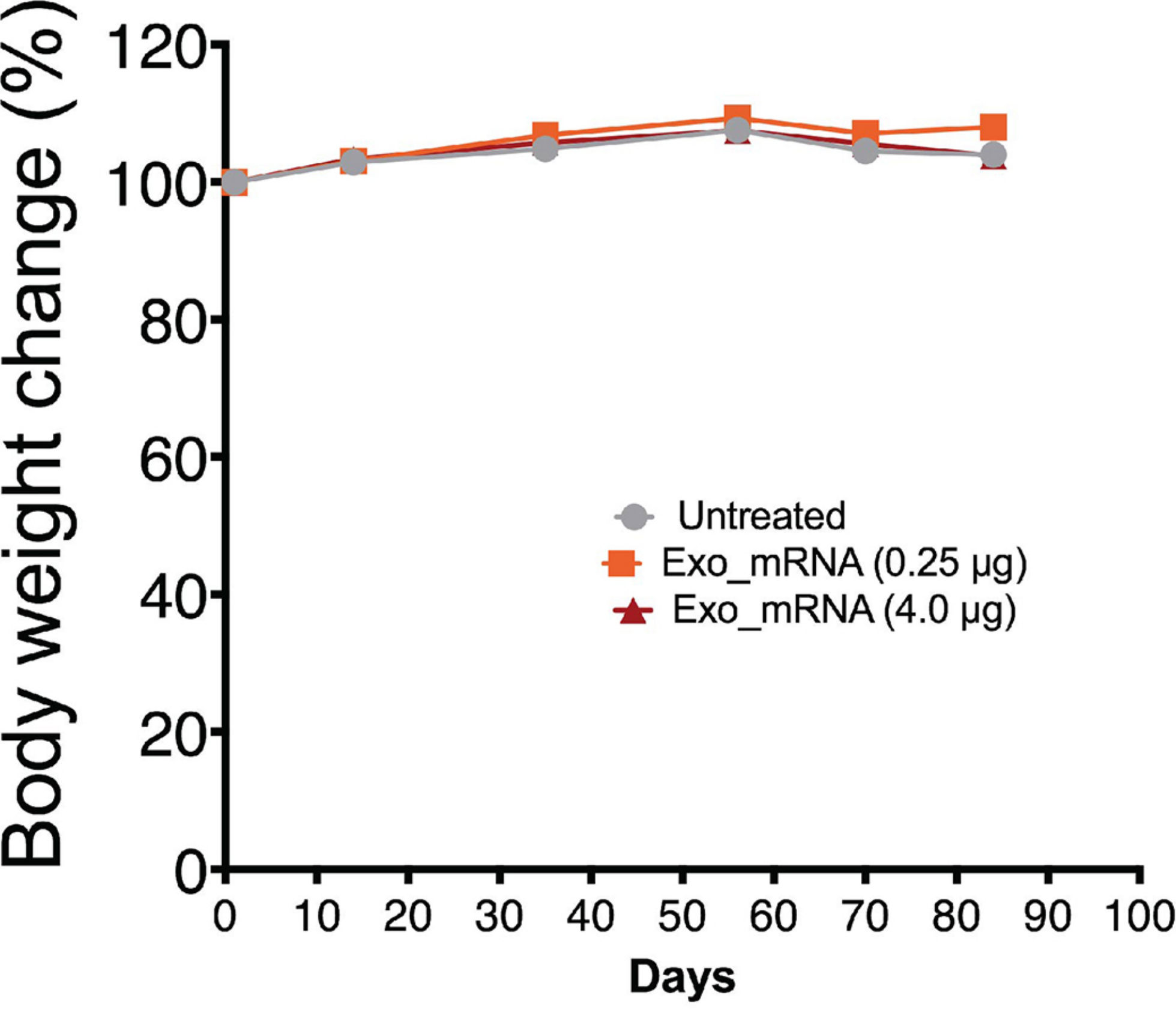

Supplemental Figure 1

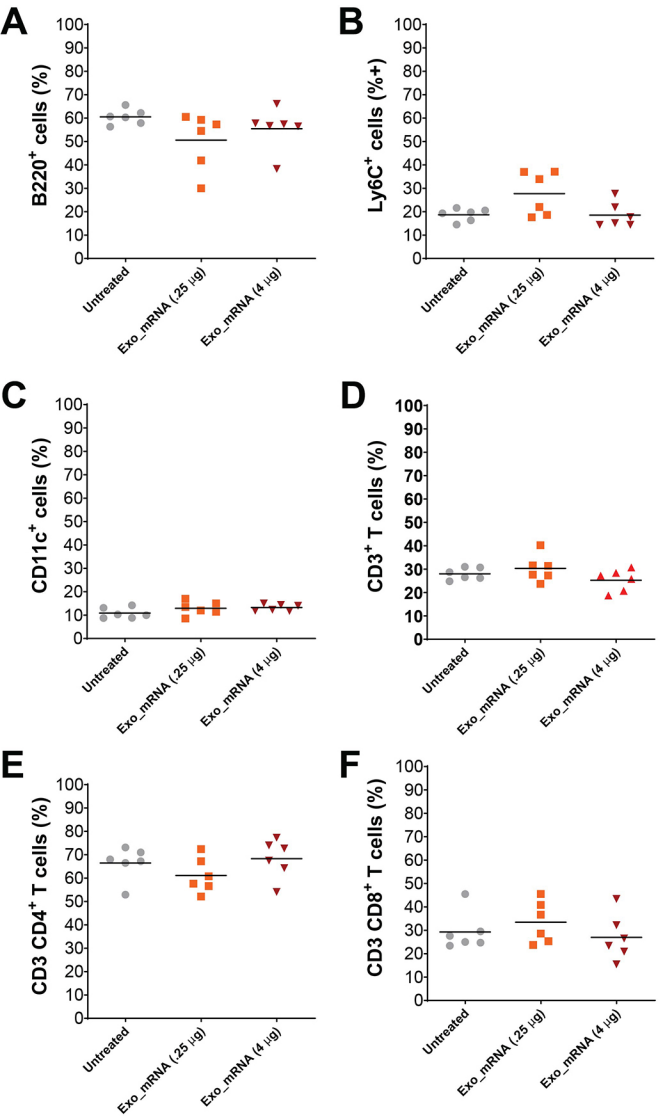

Supplemental Figure 2